Research Article

Characteristics of neural growth and cryopreservation of the dorsal root ganglion using three-dimensional collagen hydrogel culture *versus* conventional culture

https://doi.org/10.4103/1673-5374.306097

Date of submission: October 14, 2020

Date of decision: November 16, 2020

Date of acceptance: December 25, 2020

Date of web publication: January 25, 2021

Ze-Kai Cui[1, 2, 3], Shen-Yang Li[3], Kai Liao[3], Zhi-Jie Wang[3], Yong-Long Guo[4, 5, 6], Luo-Sheng Tang[1], Shi-Bo Tang[2, 3, 7], Jacey Hongjie Ma[1, 2, 8, *], Jian-Su Chen[2, 3, 4, 5, 6, *]

Graphical Abstract *In vitro culture of DRG in collagen gel provides a promising approach for 3D culture, cryopreservation, and transplantation of DRG.*

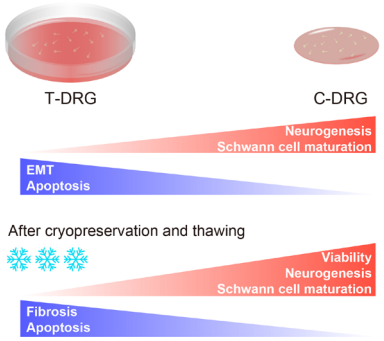

Abstract

In vertebrates, most somatosensory pathways begin with the activation of dorsal root ganglion (DRG) neurons. The development of an appropriate DRG culture method is a prerequisite for establishing *in vitro* peripheral nerve disease models and for screening therapeutic drugs. In this study, we compared the changes in morphology, molecular biology, and transcriptomics of chicken embryo DRG cultured on tissue culture plates (T-DRG) *versus* three-dimensional collagen hydrogels (C-DRG). Our results showed that after 7 days of culture, the transcriptomics of T-DRG and C-DRG were quite different. The upregulated genes in C-DRG were mainly related to neurogenesis, axon guidance, and synaptic plasticity, whereas the downregulated genes in C-DRG were mainly related to cell proliferation and cell division. In addition, the genes related to cycles/pathways such as the synaptic vesicle cycle, cyclic adenosine monophosphate signaling pathway, and calcium signaling pathway were activated, while those related to cell-cycle pathways were downregulated. Furthermore, neurogenesis- and myelination-related genes were highly expressed in C-DRG, while epithelial–mesenchymal transition-, apoptosis-, and cell division-related genes were suppressed. Morphological results indicated that the numbers of branches, junctions, and end-point voxels per C-DRG were significantly greater than those per T-DRG. Furthermore, cells were scattered in T-DRG and more concentrated in C-DRG, with a higher ratio of 5-ethynyl-2′-deoxyuridine (EdU)-positive cells in T-DRG compared with C-DRG. C-DRG also had higher S100 calcium-binding protein B (S100B) and lower α-smooth muscle actin (α-SMA) expression than T-DRG, and contained fewer terminal deoxynucleotidyl transferase dUTP nick end labeling (TUNEL)-positive cells after 48 hours of serum starvation. After cryopreservation, C-DRG maintained more intact morphological characteristics, and had higher viability and less TUNEL-positive cells than T-DRG. Furthermore, newly formed nerve bundles were able to grow along the existing Schwann cells in C-DRG. These results suggest that C-DRG may be a promising *in vitro* culture model, with better nerve growth and anti-apoptotic ability, quiescent Schwann cells, and higher viability. Results from this study provide a reference for the construction, storage, and transportation of tissue-engineered nerves. The study was approved by the Ethics Committee of Aier School of Ophthalmology, Central South University, China (approval No. 2020-IRB16), on March 15, 2020.

Key Words: anti-apoptosis; collagen hydrogel; cryopreservation; dorsal root ganglion; neurogenesis; RNA-seq; Schwann cell; tissue engineering

Chinese Library Classification No. R452; R741; Q813.1+1

[1]Department of Ophthalmology, the Second Xiangya Hospital, Central South University, Changsha, Hunan Province, China; [2]Aier Eye Institute, Changsha, Hunan Province, China; [3]Aier School of Ophthalmology, Central South University, Changsha, Hunan Province, China; [4]Institute of Ophthalmology, Medical College, Jinan University, Guangzhou, Guangdong Province, China; [5]Department of Ophthalmology, First Affiliated Hospital of Jinan University, Guangzhou, Guangdong Province, China; [6]Key Laboratory for Regenerative Medicine of Ministry of Education, Jinan University, Guangzhou, Guangdong Province, China; [7]CAS Center for Excellence in Brain Science and Intelligence Technology, Chinese Academy of Sciences, Shanghai, China; [8]Imaging and Functional Center, Guangzhou Aier Eye Hospital, Guangzhou, Guangdong Province, China

***Correspondence to:** Jian-Su Chen, MD, PhD, chenjiansu2000@163.com; Jacey Hongjie Ma, MD, PhD, ma.hongjie12@gmail.com.

https://orcid.org/0000-0003-3670-6219 (Ze-Kai Cui)

Funding: *This study was supported by the National Natural Science Foundation of China, Nos. 82000871 (to ZKC), 81871495 (to JSC); the Natural Science Foundation of Hunan Province, China, No. 2020JJ5001 (to ZKC); the Science Research Grant of Aier Eye Hospital Group, China, No. AF1913D2 (to ZKC), and Central South University Postdoctoral Funds, China.*

How to cite this article: *Cui ZK, Li SY, Liao K, Wang ZJ, Guo YL, Tang LS, Tang SB, Ma JH, Chen JS (2021) Characteristics of neural growth and cryopreservation of the dorsal root ganglion using three-dimensional collagen hydrogel culture versus conventional culture. Neural Regen Res 16(9):1856-1864.*

Introduction

Peripheral nerve injury is one of the most important causes of disability, and has a considerable impact on the daily lives of patients (Wojtkiewicz et al., 2015). Because of the higher functional and structural complexity of the nervous system compared with other tissue in the human body, it is challenging to treat neural diseases (Gaudin et al., 2016). In vertebrates, most somatosensory pathways begin with the activation of dorsal root ganglion (DRG) neurons, which are responsible for thermoception, nociception, mechanoreception, and proprioception (Nascimento et al., 2018; Puopolo, 2019). Consequently, the *in vitro* study of DRG is important for modeling peripheral nerve diseases and screening therapeutic drugs. To develop and evaluate regeneration strategies for nerve repair, appropriate preclinical models are needed that effectively mimic the microenvironment of nerve damage and regeneration. For decades, there have been many studies using two-dimensional (2D) neuronal cultures. The 2D culture model provides a relatively stable culture environment and is easy to manipulate and observe. However, the major limitation of these systems is their failure to recapitulate *in vivo* cell-cell and cell-matrix interactions. For many 2D cell culture models, there is questionable accuracy for reproducing *in vivo* cell behavior (Mobini et al., 2019). In addition, glass or plastic tissue culture plates (TCPs) are often used in traditional 2D cell culture. These materials are several orders of magnitude stiffer than nerve tissue in the body (Hopkins et al., 2013). Changes in the mechanical properties of substrates affect cell morphology, gene expression, and proliferation (East et al., 2009; Balasubramanian et al., 2016), and the behavior of nerve cells cultured in 2D TCPs differs from that in three-dimensional (3D) culture and *in vivo* (Pardo and Honegger, 2000; Peretz et al., 2007). Currently, the general consensus is that 3D *in vitro* culture is more physiologically relevant than 2D culture, because the former can reproduce an *in vivo*-like structure and extracellular microenvironment. In contrast to 2D culture, which is spatially limited, cells in 3D culture can grow and migrate in any direction, thus simulating neural network structures *in vitro* (Mobini et al., 2019). Today, 3D culture is one of the most important configurations of neuronal cultures *in vitro* (Gu et al., 2018). Recently, Moxon et al. (2019) encapsulated human induced pluripotent stem cell-derived neurons in alginate/collagen hydrogels, and found that the encapsulated neurons formed a complex neural network. Furthermore, the 3D hydrogel scaffolds promoted the key processes of neuronal maturation and synapse formation (Moxon et al., 2019). Additionally, Malheiro et al. (2020) used electrospun scaffolds and fibrin hydrogels to build an interactive platform between mouse DRG and Schwann cells. The addition of exogenous Schwann cells enhanced neurite length and the area of neurite growth. This platform may eventually replace animal models for drug testing (Malheiro et al., 2020). In another study, Wang et al. (2017) seeded DRG in silk sponge to simulate limbal nerve growth. After 28 days of culture, nerves had innervated the tissue-engineered corneal epithelium. This finding provides a model for studying corneal development *in vitro* (Wang et al., 2017).

Cryopreservation can slow down or stop the metabolism and cellular processes, thereby preserving living cells for a long time. This process is crucial after tissue dissection and dissociation, because preserving excess cells allows us to make full use of precious animal and human samples. Cryopreservation of unused primary cells also increases the cost efficiency of primary cell isolation, reduces the frequency of cell isolation, and improves utilization rates (Otto et al., 2003). Despite the optimization of freezing parameters and medium composition, the long-term survival rate of neurons stored using these methods remain low (Higgins et al., 2011; Robert et al., 2016), making neuronal cryopreservation an inefficient practice. Previous studies have reported that DRG neurons exhibit low cell viability after cryopreservation (Seggio et al., 2008; Schwarz et al., 2019).

In the present study, we aimed to analyze the effects of collagen hydrogel encapsulation on the growth and cryopreservation of DRG. We constructed a DRG-laden collagen hydrogel (C-DRG) and evaluated the differences between C-DRG and traditional 2D TCP DRG cultures (T-DRG), based on the cell morphology, transcriptome, proliferation, apoptosis, and expression of biomarkers of neurons and Schwann cells. After cryopreservation and thawing, the morphology, viability, biomarker expression, and gene expression changes of C-DRG and T-DRG were again evaluated.

Materials and Methods

Extraction of chicken embryo DRGs and construction of C-DRG

The study was approved by the Ethics Committee of Aier School of Ophthalmology, Central South University, China (approval No. 2020-IRB16), on March 15, 2020. The animals were treated in accordance with the Guide for the Care and Use of Animals (DHEW Publication, NIH, 80-23). One hundred fertilized chicken eggs were purchased from Hanshan Ecological Farm (Suqian, China). The fertilized eggs were kept in an incubator (37.8°C, relative humidity 80%) for 7–9 days. Chicken embryo DRGs were harvested from embryonic day (E)7–9 chicken embryos, based on a previous study (Powell et al., 2014). For the T-DRG group, the isolated DRGs were seeded in a 12-well plate, with 15 DRGs per well. The culture plate was coated with poly-D-lysine solution (100 ng/mL, Sigma-Aldrich, St. Louis, MO, USA) at 4°C for 12 hours in advance. For the C-DRG group, C-DRG was constructed according to our previous study (Cui et al., 2018). Briefly, 15 DRGs were collected in a centrifuge tube. The tube was mixed after adding 0.9 mL 0.5% pre-cooled type I collagen solution (extracted from bovine tendon, Guangzhou Trauer Biotechnology, Guangzhou, China) and 0.1 mL 10× Dulbecco's modified Eagle medium (DMEM; Hyclone Laboratories, Logan, UT, USA). After centrifuging to remove bubbles, the collagen solution containing DRGs was transferred to a 12-well plate. The plate was incubated at 37°C for 30 minutes to allow the collagen hydrogel to fully solidify. Finally, T-DRG and C-DRG were cultured in DMEM/F12 (Gibco, Grand Island, NY, USA) supplemented with 5% fetal bovine serum (FBS; Gibco), 100 mg/mL penicillin, 100 mg/mL streptomycin (Gibco) and 50 ng/mL nerve growth factor 2.5S Native Mouse Protein (Gibco) at 37°C, 5% CO_2 for 7 days.

Cryopreservation and thawing

The cryopreservation of DRG was performed according to a previous study, with slight modifications (Schwarz et al., 2019). T-DRG and C-DRG were collected in cryovials (Thermo Fisher Scientific, Waltham, MA, USA) with 1 mL freezing medium containing 10% dimethyl sulfoxide (MP Biomedicals, Irvine, CA, USA), 30% FBS (Life Technologies, Carlsbad, CA), and 60% DMEM/F12 (Life Technologies). The cryovials were then placed into a freezing container and cooled to –80°C. They were placed into liquid nitrogen after 24 hours (–196°C). After 1 week, the cryovials were thawed at 37°C, and the content of the T-DRG or C-DRG cryovials was transferred to culture plates and washed three times with DMEM/F12 containing 5% FBS. The T-DRG, C-DRGs or hydrogels were transferred to 12-well plates pre-coated with poly-D-lysine, and were then cultured in DMEM/F12 (Life Technologies) supplemented with 5% FBS (Life Technologies), 100 mg/mL penicillin, 100 mg/mL streptomycin (Life Technologies), and 50 ng/mL nerve growth factor 2.5S Native Mouse Protein (Thermo Fisher) at 37°C, 5% CO_2 for 7 days.

Immunofluorescent staining

Samples of T-DRG, C-DRG, cryo-T-DRG, and cryo-C-DRG were

fixed using 4% paraformaldehyde at room temperature for 15 minutes. After three rinses with phosphate-buffered saline (PBS), they were immersed in the blocking and permeabilizing solution, supplemented with 3% bovine serum albumin (BSA) and 1% Triton-X 100, for 1 hour at room temperature. The primary antibodies (mouse monoclonal anti-βIII-tubulin, Cat# ab78078, 1:1000, Abcam, Cambridge, UK; rabbit polyclonal anti-S100 calcium-binding protein B [S100B], Cat# bs-2015R, 1:500, Bioss, Beijing, China; and rabbit polyclonal anti-alpha smooth muscle actin [α-SMA], Cat# bs-0189R, 1:500, Bioss) were added to the solution, and the samples were incubated overnight at 4°C. After three rinses with PBS, the samples were incubated in 1% BSA solution with secondary antibodies diluted at 1:1000 (goat anti-rabbit/mouse IgG Alexa Fluor 488/594/647, Cat# A-11034/A-11005/A-21244, Invitrogen, Carlsbad, CA, USA) for 1 hour at room temperature. Cell nuclei were then stained with 4′,6-diamidino-2-phenylindole (DAPI). After rinsing three times with PBS, the samples were imaged using laser scanning confocal microscopy (LSM 800, Zeiss, Jena, Germany).

RNA sequencing analysis

Total RNA was extracted from T-DRG and C-DRG, with samples collected from three repeated experiments for each group. RNA sequencing (RNA-seq) was performed by Chi Biotech Co., Ltd. (Shenzhen, China). The RNA of samples was then submitted for the library construction. The correlation coefficient and principal component analyses between groups were calculated and plotted. After library sequencing and mapping, the R package edgeR (3.26.8) (www.r-project.org) was used to normalize and screen differentially expressed genes (DEGs). The screening threshold was set to |log2 (fold change)| > 1 and false discovery rate < 0.05. Gene ontology (GO) and Kyoto Encyclopedia of Genes and Genomes (KEGG) enrichment analysis was performed using Metascape (www.metascape.org) (Zhou et al., 2019). Diagrams were plotted using the R packages ggplot2 (3.2.1), pheatmap (1.0.12), and circlize (0.4.8) (www.r-project.org).

5-Ethynyl-2′-deoxyuridine labeling

For 5-ethynyl-2′-deoxyuridine (EdU) labeling in T-DRG and C-DRG, we used the Click-iT EdU Alexa Fluor 488 Imaging Kit (KeyGEN Biotechnology, Nanjing, China) according to the manufacturer's recommendations. Briefly, EdU was added to culture medium (10 μM) for 4 hours. The samples were then fixed using 4% paraformaldehyde for 15 minutes at room temperature. Next, they were immersed in the blocking and permeabilizing solution, supplemented with 3% BSA and 1% Triton-X 100, for 1 hour at room temperature. After three washes, the samples were treated for 15 minutes with a Click-iT cocktail containing Alexa Fluor 488 azide. DAPI was used to stain cell nuclei, and the samples were imaged using laser scanning confocal microscopy (LSM 800).

Terminal deoxynucleotidyl transferase dUTP nick-end labeling staining

After serum starvation or cryopreservation, cellular apoptosis in T-DRG and C-DRG was analyzed using the One Step terminal deoxynucleotidyl transferase dUTP nick-end labeling (TUNEL) Apoptosis Assay Kit (Beyotime Biotechnology, Shanghai, China) according to the manufacturer's recommendations. Samples were first fixed using 4% paraformaldehyde at room temperature for 15 minutes. They were then immersed in the blocking and permeabilizing solution, supplemented with 3% BSA and 1% Triton-X 100, for 1 hour at room temperature. Samples were then incubated with TUNEL assay solution for 1 hour at 37°C. Next, DAPI was used to stain cell nuclei, and the samples were imaged using laser scanning confocal microscopy (LSM 800).

Quantitative real-time polymerase chain reaction

RNA was extracted from T-DRG and C-DRG using TRIzol Reagent (Thermo Fisher). Three biological replicates were analyzed for each group. The RNA was reverse transcribed into complementary DNA using HiScript® II Reverse Transcriptase (Vazyme, Nanjing, China). Each qPCR sample, in 10 μL of total volume, contained 5 μL of 2× SYBR (Vazyme), 250 nM of forward and reverse primers, and 10 ng of complementary DNA. The primers were designed using Primer-BLAST (www.ncbi.nlm.nih.gov). The primers are listed in **Additional Table 1**. Quantitative real-time polymerase chain reaction (qPCR) was performed using the LightCycler96 (Roche, Basel, Switzerland). The results of each amplification were normalized to the glyceraldehyde-3-phosphate-dehydrogenase (GAPDH) mRNA transcript.

Statistical analysis

Data are represented as the mean ± standard deviation (SD). The Student's *t*-test was performed to compare between groups using GraphPad 8.0 (GraphPad Software, Inc., La Jolla, CA, USA). $P < 0.05$ was considered significant. The fluorescence intensity, cell counting, and skeleton analyses were performed using Fiji/ImageJ (National Institutes of Health, Bethesda, MD, USA).

Results

Growth of T-DRG and C-DRG and their transcriptomic differences

We harvested DRG from E7–9 chicken embryos and seeded them in TCP or collagen hydrogel, respectively, for T-DRG and C-DRG. The experimental protocol is shown in **Figure 1**. After 7 days of culture, we observed the extension of nerve bundles in both T-DRG and C-DRG. The nerve bundles in C-DRG were denser than those in T-DRG.

We then extracted RNA from T-DRG and C-DRG for transcriptomic analysis. The original read count data are shown in **Additional Table 2**. A Pearson correlation heatmap and principal component analysis plot revealed that both T-DRG and C-DRG samples had good biological reproducibility (**Additional Figure 1**). T-DRG was considered the control group. In the C-DRG group, 1866 genes were upregulated and 1154 genes were downregulated. We labeled the 30 DEGs that had the highest counts per million (**Figure 2A**). Among these DEGs, downregulated genes were related to extracellular matrix (ECM) organization and actin cytoskeleton organization, while upregulated genes were related to processes such as axonogenesis and synaptic plasticity (**Figure 2B**). We performed GO biological process enrichment on all DEGs, and selected the top 15 GO terms with the largest significances. Compared with the T-DRG group, the upregulated terms in C-DRG included synapse organization, axonogenesis, axon development, cell morphogenesis involved in neuron differentiation, and synaptic signaling. The downregulated terms included mitotic nuclear division, ECM organization, nuclear division, extracellular structure organization, and cell cycle G_2/M phase transition (**Figure 2C**). In the KEGG analysis, the 15 signaling pathways that were most significantly different between the C-DRG and T-DRG groups are shown in **Figure 2D**. Cell cycle-related genes were the most downregulated, while genes related to the synaptic vesicle cycle, retrograde endocannabinoid signaling, MAPK signaling pathway, neuroactive ligand–receptor interaction, cAMP signaling pathway, and calcium signaling pathway were upregulated. In particular, ECM–receptor interaction had the highest-fold enrichment. All results of the DEGs and the GO and KEGG enrichment analyses are listed in **Additional Tables 3–5**.

Our results indicate that, compared with T-DRG, C-DRG has higher expression of neurogenesis-related genes, while proliferation-related genes are downregulated. Overall, the two groups demonstrated significant transcriptomic differences.

Compared with T-DRG, C-DRG exhibits denser nerve bundles

To compare the morphological characteristics of DRG in TCPs and collagen gel, we performed immunofluorescence staining of T-DRG and C-DRG after 7 days of culture. Neurons were labeled with βIII-tubulin antibodies (Varderidou-Minasian et al., 2020). The nerve bundles of T-DRG were thicker and sparser, while those of C-DRG were thinner and denser (**Figures 1B** and **3A**). The images were skeletonized and quantitatively analyzed (n = 15). The number of branches per C-DRG was significantly larger than that per T-DRG (38 230 ± 20 987 *vs*. 6384 ± 2615, P < 0.001) (**Figure 3B**). Similarly, the number of junctions per C-DRG was markedly larger than that per T-DRG (17 843 ± 11 239 *vs*. 3418 ± 1311, P < 0.001) (**Figure 3C**). There were also more end-point voxels per C-DRG than T-DRG (8674 ± 4254 *vs*. 1939 ± 678, P < 0.001) (**Figure 3D**). Moreover, the average branch length per C-DRG was much shorter than that per T-DRG (16.2 ± 2.0 μm *vs*. 32.4 ± 4.7 μm, P < 0.001) (**Figure 3E**). We selected axon guidance-related DEGs for heatmap plotting (**Figure 3F**). The resulting plot revealed that, compared with the T-DRG group, most DEGs in axon guidance were upregulated in the C-DRG group (especially GAP43 and TUBB3). The qPCR results verified that the axon guidance- and axonogenesis-related genes TUBB3, GAP43, NEFM, and NEFL were significantly upregulated (**Figure 3G**). These results suggest that C-DRG has a denser nerve bundle than T-DRG.

C-DRG demonstrates higher expression of Schwann cell biomarkers and lower degrees of proliferation, apoptosis, and fibrosis compared with T-DRG

To evaluate the proliferation and expression of Schwann cell biomarkers in T-DRG and C-DRG, we performed immunofluorescence staining. Our results revealed that the migration ability of Schwann cells in C-DRG was lower than that in T-DRG. Cells were therefore more scattered in T-DRG and more concentrated in C-DRG (**Figure 4A** and **B**). Additionally, the fluorescent density of the Schwann cell marker S100B (Tucker et al., 2011) in T-DRG was significantly lower than in C-DRG (P < 0.01) (**Figure 4A** and **C**). Furthermore, T-DRG expressed a large amount of the fibrotic marker α-SMA (Lan et al., 2018), and α-SMA expression was significantly lower in C-DRG (P < 0.05) (**Figure 4B** and **C**). The ratio of EdU-positive cells in C-DRG was markedly lower than that in T-DRG (0.094 ± 0.014 *vs*. 0.298 ± 0.051, P < 0.001) (**Figure 4D**). Moreover, RNA-seq heatmaps showed that, compared with the T-DRG group, DEGs involved in the positive regulation of epithelial-mesenchymal transition (EMT) and the regulation of mitotic nuclear division were downregulated in the C-DRG group. In contrast, myelination-related DEGs were upregulated in the C-DRG group (especially S100B and NRG1) (**Figure 4E**). The qPCR results also showed that the Schwann cell-related genes S100B and NRG1 were upregulated in C-DRG compared with T-DRG, while the proliferation-related genes MKI67 and PCNA were downregulated. The EMT transcription factor ZEB1 was significantly downregulated (**Figure 4F**).

To evaluate the anti-apoptotic abilities of T-DRG and C-DRG Schwann cells, we performed serum starvation. After 48 hours of serum withdrawal, apoptotic cells were labeled using TUNEL. Most TUNEL-positive cells were Schwann cells (**Figure 5A**). The ratio of TUNEL-positive cells in C-DRG was significantly lower than that in T-DRG (0.073 ± 0.019 *vs*. 0.422 ± 0.201, P < 0.01) (**Figure 5B**). DEGs related to the apoptotic process were also downregulated (**Figure 5C**). Moreover, qPCR revealed that the apoptosis-related genes FAS, CASP2, and FADD were significantly downregulated in C-DRG compared with T-DRG (**Figure 5D**).

These results suggest that, compared with T-DRG, C-DRG has higher expression of Schwann cell biomarkers and better anti-apoptotic ability. In addition, C-DRG showed lower degrees of fibrosis and proliferation. These findings indicate that Schwann cells may have quiescent characteristics in collagen scaffolds.

After cryopreservation and thawing, C-DRG has denser nerve bundles and better viability than T-DRG

After cryopreservation and thawing, T-DRG and C-DRG were cultured for 7 days (cryo-T-DRG and cryo-C-DRG, respectively). We performed a morphological analysis of cryo-T-DRG and cryo-C-DRG. Neurons were labeled with βIII-tubulin antibody. Similar to pre-cryopreservation, the nerve bundles of cryo-T-DRG were thicker and sparser, whereas the nerve bundles of cryo-C-DRG were thinner and denser (**Figure 6A**). The images were skeletonized and quantitatively analyzed [n(cryo-T-DRG) = 16, n(cryo-T-DRG) = 12]. The number of branches per cryo-C-DRG was significantly greater than that per cryo-T-DRG (3422 ± 1265 *vs*. 1300 ± 1326, P < 0.001) (**Figure 6B**). Similarly, the number of junctions per cryo-C-DRG was markedly higher than that per cryo-T-DRG (1505 ± 659 *vs*. 683 ± 727, P < 0.01) (**Figure 6C**). There were also more end-point voxels per cryo-C-DRG than per cryo-T-DRG (896 ± 318 *vs*. 331 ± 299, P < 0.001) (**Figure 6D**). Finally, the average branch length per cryo-C-DRG was much shorter than that per cryo-T-DRG (18.6 ± 4.2 μm *vs*. 36.5 ± 3.1 μm, P < 0.001) (**Figure 6E**). Overall, compared with pre-cryopreservation, the values of these indicators were lower after thawing. The viability of cryo-C-DRG was also higher than that of cryo-T-DRG (84.2 ± 4.0% *vs*. 46.3 ± 1.6%, P < 0.001) (**Figure 6F**). Our results therefore revealed that cryo-C-DRG have a denser nerve bundle and better viability compared with cryo-T-DRG.

Cryo-C-DRG has a higher expression of Schwann cell biomarkers and a lower degree of apoptosis than cryo-T-DRG

To evaluate the expression of Schwann cell biomarkers in cryo-T-DRG and cryo-C-DRG, we performed immunofluorescence staining. Apoptotic cells were labeled with TUNEL. The ratio of TUNEL-positive cells in cryo-T-DRG was significantly higher than in cryo-C-DRG (P < 0.05) (**Figure 7A** and **B**). In addition, compared with cryo-T-DRG, cryo-C-DRG had significantly higher S100B fluorescent density (P < 0.001) (**Figure 7A** and **C**). We also observed that the nerve bundles of cryo-C-DRG disintegrated after being damaged by low temperatures, but Schwann cells remained present, and the newly formed nerve bundles were able to grow along the existing Schwann cells, which functioned as axon guidance. On day 2 after thawing, newly formed nerve bundles appeared and began to slowly extend in the direction of existing Schwann cells. On day 7 after thawing, newly formed nerve bundles mostly overlapped with the existing Schwann cells (**Figure 7D**). The qPCR results revealed that, compared with cryo-T-DRG, the Schwann cell-related genes *S100B* and *NRG1* were upregulated in cryo-C-DRG. The axon guidance- and axonogenesis-related genes *TUBB3*, *GAP43*, *NEFM*, and *NEFL*, as well as the proliferation-related gene *PCNA*, were also significantly upregulated in cryo-C-DRG. In contrast, the fibrosis-related genes *ACTA2* and *FN1* and the apoptosis-related gene *FAS* were downregulated compared with cryo-T-DRG. Finally, the neurodevelopmental transcription factor gene *TCF3* was upregulated in cryo-C-DRG (**Figure 7E**). Compared with pre-cryopreservation, both cryo-T-DRG and cryo-C-DRG had downregulation of proliferation-related genes and of biomarker genes of Schwann cells and neurons; in contrast, genes for transcription factors involved in fibrosis, apoptosis, and neurodevelopment were upregulated (**Figure 7F**). The detailed qPCR statistics are displayed in **Additional Figure 2**.

These results suggest that, compared with cryo-T-DRG, cryo-C-DRG has higher expression of Schwann cell and neuron biomarkers, and a lower degree of apoptosis and fibrosis. These findings imply that cryo-C-DRG may have stronger nerve regeneration potential.

Discussion

Traditional 2D cell culture is simple and convenient to analyze, but the specific tissue structure, mechanical and biochemical cues, and cellular communication are often missing. This can result in questionable models for disease modeling and preclinical drug screening (Murphy et al., 2017). The 3D cell culture system aims to overcome these limitations by replicating the *in situ* function of living tissue, thus providing more physiologically relevant environments for cell growth and function. For tissue-engineered nerves to truly represent nerve tissue in the central and peripheral nervous systems, a scaffold is needed to reconstruct the 3D physiological microenvironment *in vitro*. In the current study, we used collagen hydrogel as a scaffold for the 3D culture of chicken embryo DRG. The DRG nerve bundles in the collagen scaffold were denser than those in 2D TCP culture. Additionally, transcriptomic analysis showed marked changes in signaling pathways. Among these, a higher ratio of upregulated DEGs in C-DRG were related to the synaptic vesicle cycle, cAMP signaling pathway, and calcium signaling pathway. The enhancement of these pathways has been reported to improve nerve growth and development (de Faria Poloni et al., 2011; Podda and Grassi, 2014). In addition, significant differences in genes associated with ECM-related pathways (focal adhesion, ECM-receptor interaction) have previously illustrated the effects of different ECM on nerve growth (Song and Dityatev, 2018). A similar phenomenon was also observed by Ribeiro et al. (2012): DRG neurons exhibited more branches and longer neurites when cultured in collagen hydrogel. These authors also revealed that the percentage of DRG neurons with a single primary neurite was higher in 3D collagen gels than in 2D ones (Ribeiro et al., 2012). The nerves cultivated in 3D hydrogels were also excitable. Furthermore, Zafeiriou et al. (2020) were able to induce the directed self-organization of human induced pluripotent stem cells in collagen hydrogel, to differentiate them into bioengineered neural organoids. After 40 days of culture, polarity switching and neuronal excitability were detected (Zafeiriou et al., 2020). Tay et al. (2018) developed a magnetic hyaluronic acid (HA) hydrogel that offers noninvasive neuromodulation via magneto-mechanical stimulation of primary DRG neurons. Excitability changes have been detected in neurons after mechanical stimulation (Tay et al., 2018).

In the present study, we used collagen hydrogel as a scaffold

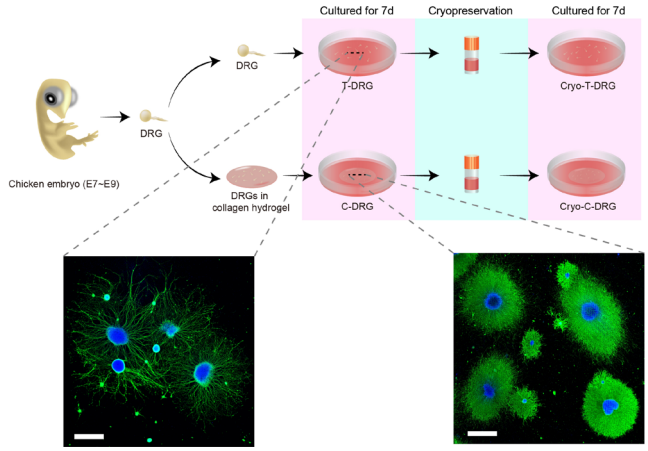

Figure 1 | Experimental procedures of the study and images showing the morphology of T-DRG and C-DRG.
The nerve bundles of C-DRG were denser than those of T-DRG. Scale bars: 1000 μm. DRG: Dorsal root ganglion; E: embryonic day; C-DRG: DRG cultured in collagen hydrogel; Cryo-T-DRG: T-DRG after cryopreservation; Cryo-C-DRG: C-DRG after cryopreservation; T-DRG: DRG cultured on tissue culture plates.

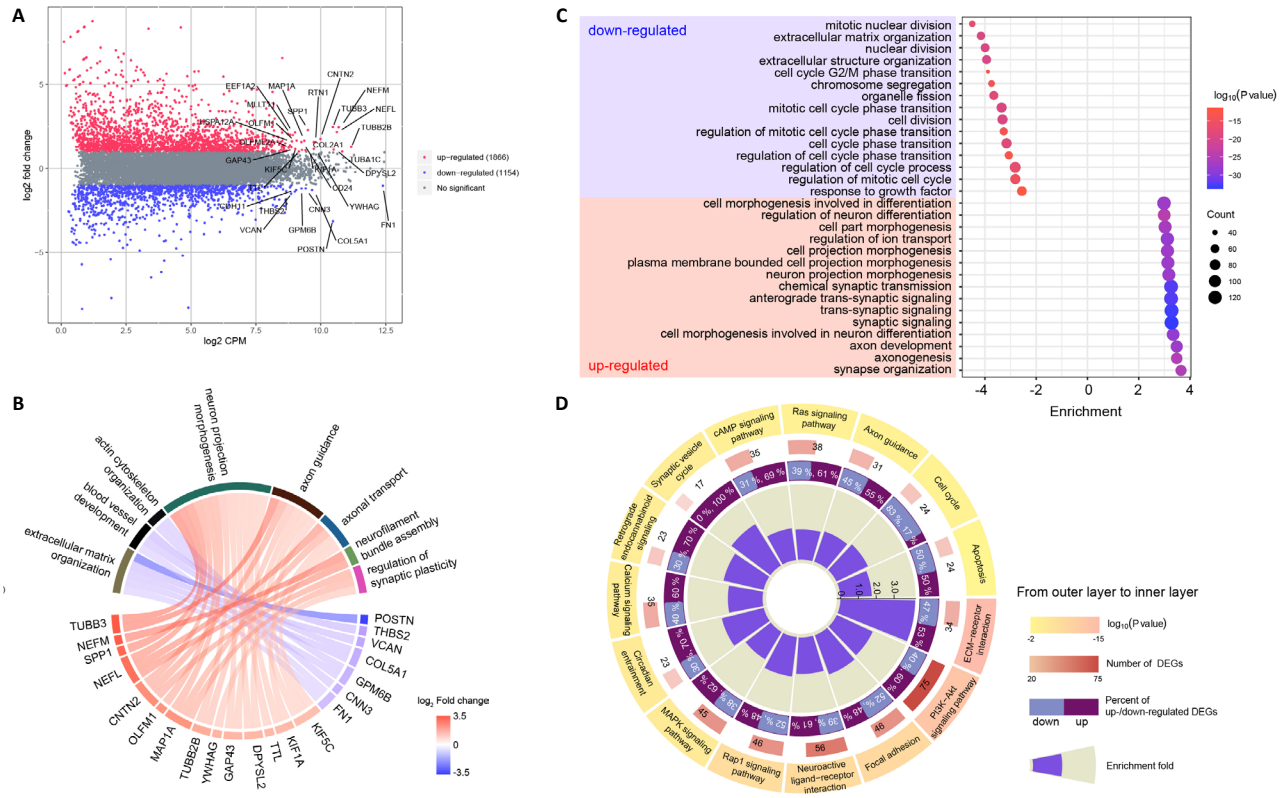

Figure 2 | RNA sequencing analysis of T-DRG and C-DRG.
T-DRG was chosen as the control group. (A) MA plot showing that 1866 genes were upregulated and 1154 genes were downregulated in the C-DRG group. The 30 DEGs with the highest CPM are labeled. (B) Circle plot revealing GO enrichment of the top 30 DEGs. (C) The top 15 GO biological process terms with the largest differences were selected. (D) The top 15 significantly changed signaling pathways in the C-DRG group are shown. From the outer to the inner layers, each layer represents the *P*-value, the number of DEGs, the percent of upregulated and downregulated DEGs, and the enrichment fold. C-DRG: Dorsal root ganglia cultured in collagen hydrogel; CPM: counts per million; DEG: differentially expressed gene; GO: gene ontology; T-DRG: dorsal root ganglia cultured on tissue culture plates.

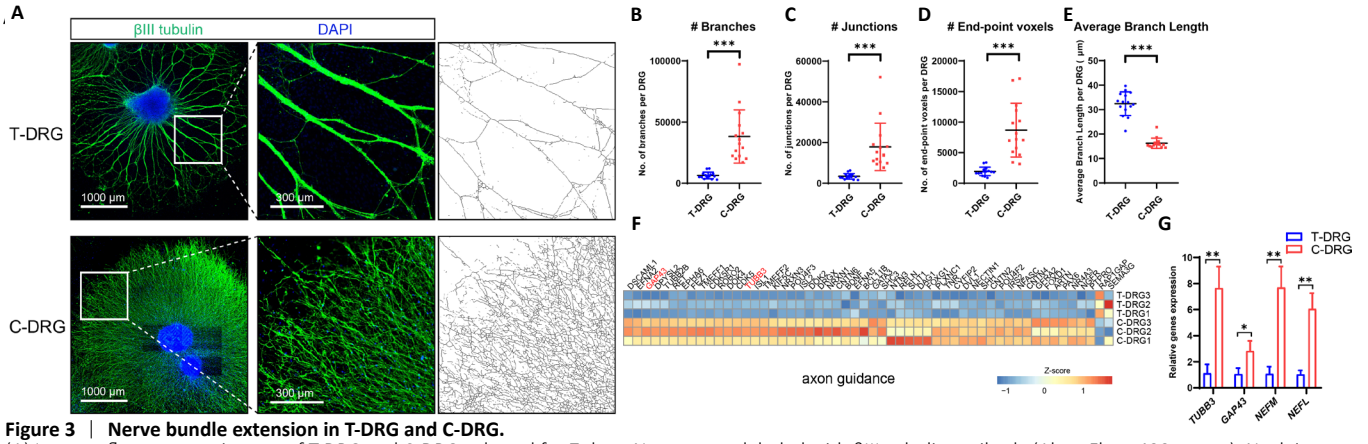

Figure 3 | Nerve bundle extension in T-DRG and C-DRG.
(A) Immunofluorescence images of T-DRG and C-DRG cultured for 7 days. Neurons are labeled with βIII-tubulin antibody (Alexa Fluor 488, green). Nuclei are labeled with DAPI (blue). Nerve bundles were skeletonized to analyze the morphological features. Compared with T-DRG, C-DRG exhibited a denser nerve bundle. Scale bars: 1000 μm, and 300 μm in the enlarged part. (B–D) The numbers of branches (B), junctions (C), and end-point voxels (D) per T-DRG or C-DRG. (E) Average branch length per T-DRG or C-DRG. (F) Heatmap of axon guidance-related DEGs. (G) The qPCR results verified the expression of axon guidance- and axonogenesis-related genes. Error bars indicate standard deviations from at least three samples. *$P < 0.05$, **$P < 0.01$, ***$P < 0.001$ (Student's *t*-test). C-DRG: Dorsal root ganglia cultured in collagen hydrogel; DAPI: 4′,6-diamidino-2-phenylindole; DEG: differentially expressed gene; DRG: dorsal root ganglion; qPCR: quantitative polymerase chain reaction; T-DRG: dorsal root ganglion cultured on tissue culture plates.

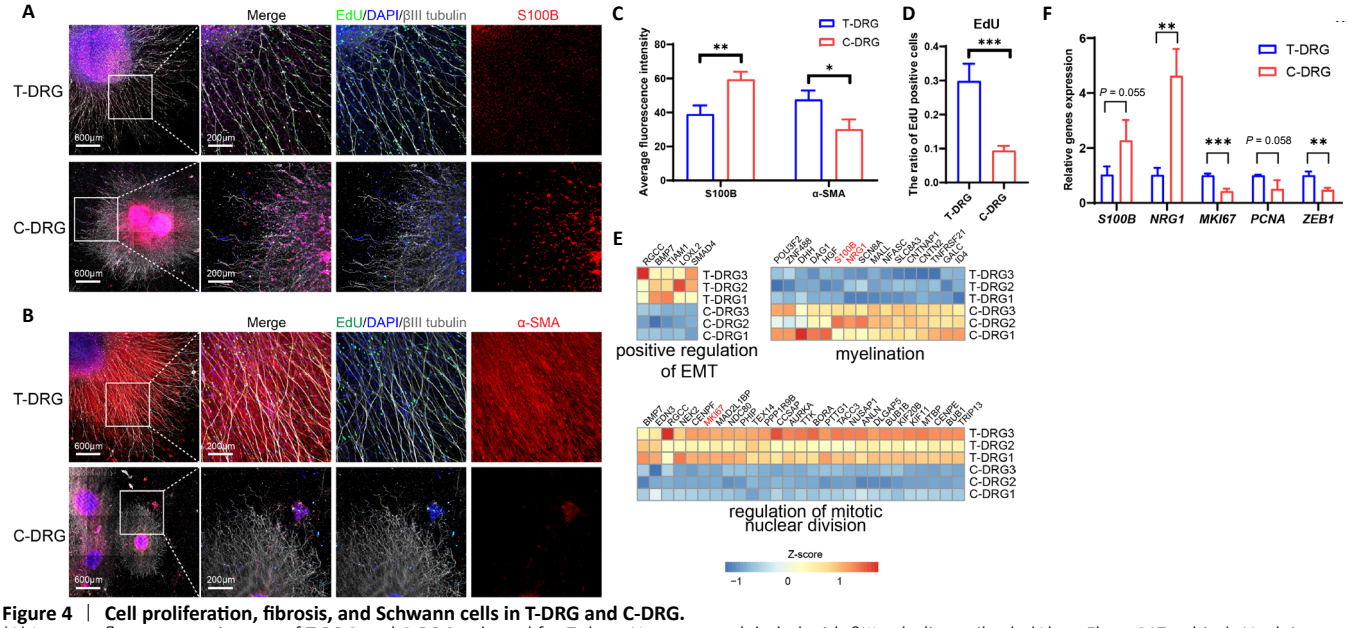

Figure 4 | Cell proliferation, fibrosis, and Schwann cells in T-DRG and C-DRG.
(A) Immunofluorescence images of T-DRG and C-DRG cultured for 7 days. Neurons are labeled with βIII-tubulin antibody (Alexa Fluor 647, white). Nuclei are labeled with DAPI (blue). Proliferating cells are labeled with EdU (Alexa Fluor 488, green). Schwann cells are labeled with S100B (Alexa Fluor 594, red). C-DRG had higher S100B expression and a lower EdU-positive ratio than T-DRG. (B) Fibrotic cells are stained by α-SMA (Alexa Fluor 594, red). T-DRG had higher expression of the fibrotic marker α-SMA compared with C-DRG. Scale bars: 600 μm, and 200 μm in the enlarged part. (C) Average fluorescence intensity of S100B and α-SMA in T-DRG and C-DRG. (D) The ratio of EdU-positive cells in T-DRG and C-DRG. (E) The heatmaps of EMT-, myelination-, and cell division-related DEGs. (F) The qPCR results verified the expression of myelination-, cell division-, and EMT-related genes. Error bars indicate standard deviations from at least three samples. *$P < 0.05$, **$P < 0.01$, ***$P < 0.001$ (Student's *t*-test). C-DRG: Dorsal root ganglia cultured in collagen hydrogel; DAPI: 4′,6-diamidino-2-phenylindole; DEG: differentially expressed gene; EdU: 5-ethynyl-2′-deoxyuridine; EMT: epithelial-mesenchymal transition; qPCR: quantitative polymerase chain reaction; T-DRG: dorsal root ganglia cultured on tissue culture plates; α-SMA: α-smooth muscle actin.

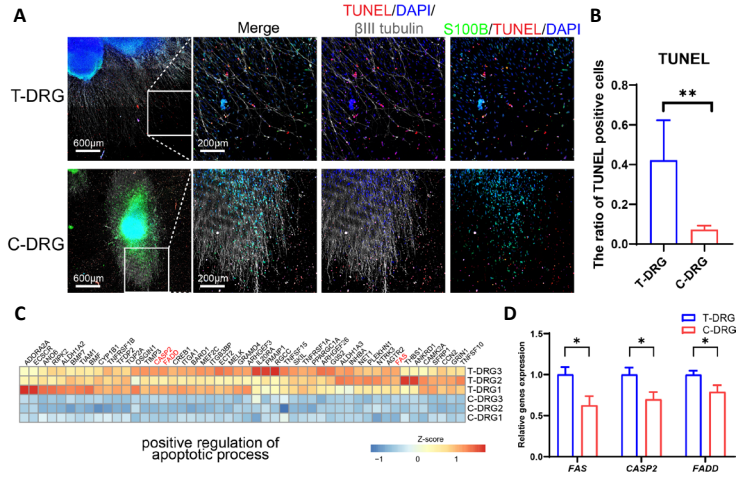

Figure 5 | Apoptosis in T-DRG and C-DRG.
(A) After 48 hours of serum withdrawal, apoptotic cells were labeled with TUNEL (Cy3, red). Nuclei are labeled with DAPI (blue). Neurons are labeled with βIII-tubulin antibody (Alexa Fluor 647, white). Schwann cells are labeled with S100B (Alexa Fluor 488, green). C-DRG had a lower TUNEL-positive ratio than T-DRG. Scale bars: 600 μm, and 200 μm in the enlarged part. (B) The ratios of TUNEL-positive cells in T-DRG and C-DRG. (C) Heatmap of apoptotic process-related DEGs. (D) The qPCR results verified the expression of apoptotic process-related genes. Error bars indicate standard deviations from at least three samples. *$P < 0.05$, **$P < 0.01$ (Student's *t*-test). C-DRG: Dorsal root ganglion cultured in collagen hydrogel; DAPI: 4′,6-diamidino-2-phenylindole; DEG: differentially expressed gene; qPCR: quantitative polymerase chain reaction; T-DRG: dorsal root ganglia cultured on tissue culture plates; TUNEL: terminal deoxynucleotidyl transferase dUTP nick-end labeling.

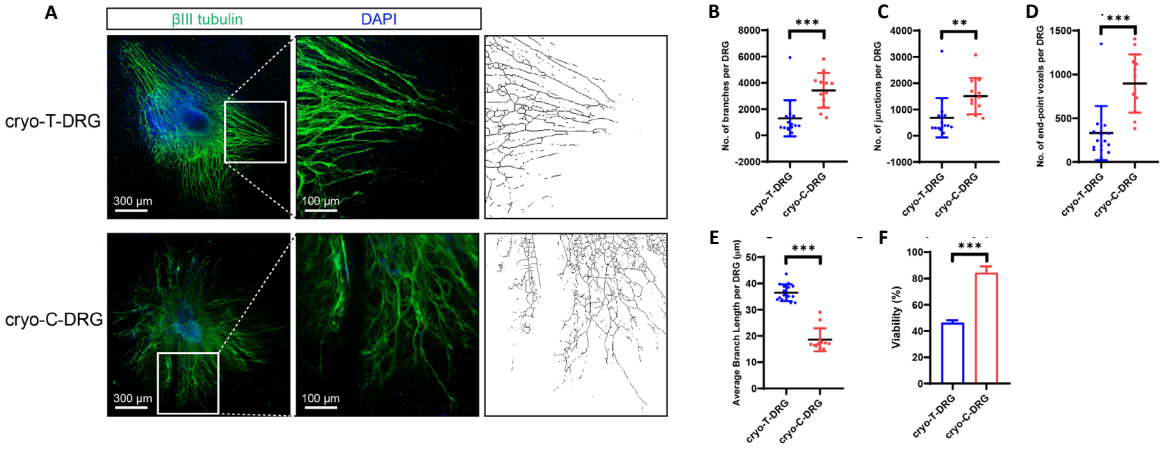

Figure 6 | **Morphological characteristics and viability of cryo-T-DRG and cryo-C-DRG.**
After cryopreservation, cryo-T-DRG and cryo-C-DRG were cultured for 7 days. (A) Immunofluorescence images of cryo-T-DRG and cryo-C-DRG. Neurons are labeled with βIII-tubulin antibody (Alexa Fluor 488, green). Nuclei are labeled with DAPI (blue). Nerve bundles were skeletonized to analyze morphological features. Compared with cryo-T-DRG, cryo-C-DRG exhibited a denser nerve bundle. Scale bars: 300 μm, and 100 μm in the enlarged part. (B–D) The numbers of branches (B), junctions (C), and end-point voxels (D) per cryo-T-DRG and cryo-C-DRG are shown. (E) Average branch length per cryo-T-DRG and cryo-C-DRG. (F) The viability of cryo-T-DRG and cryo-C-DRG. Error bars indicate standard deviations from at least three samples. $^{**}P < 0.01$, $^{***}P < 0.001$ (Student's *t*-test). C-DRG: Dorsal root ganglia cultured in collagen hydrogel; Cryo-C-DRG: C-DRG after cryopreservation; Cryo-T-DRG: T-DRG after cryopreservation; DAPI: 4′,6-diamidino-2-phenylindole; T-DRG: dorsal root ganglia cultured on tissue culture plates.

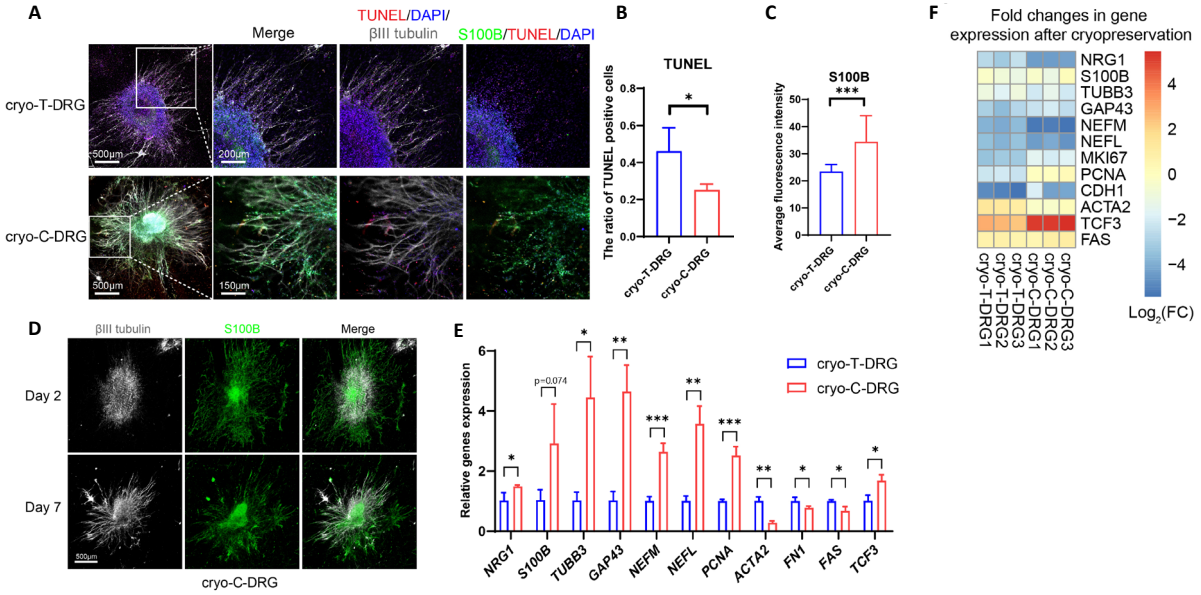

Figure 7 | **Changes in cryo-T-DRG and cryo-C-DRG after 7 days of culture.**
(A) Immunofluorescence images of cryo-T-DRG and cryo-C-DRG cultured for 7 days. Apoptotic cells are labeled with TUNEL (Cy3, red). Nuclei are labeled with DAPI (blue). Neurons are labeled with βIII-tubulin antibody (Alexa Fluor 647, white). Schwann cells are labeled with S100B (Alexa Fluor 488, green). Cryo-C-DRG had higher S100B expression and a lower TUNEL-positive ratio than cryo-T-DRG. (B) The ratio of TUNEL-positive cells in cryo-T-DRG and cryo-C-DRG. (C) Average fluorescence intensity of S100B in cryo-T-DRG and cryo-C-DRG. (D) Distribution of nerve bundles and Schwann cells in cryo-C-DRG on days 2 and 7. The newly formed nerve bundles were able to grow along the existing Schwann cells. Scale bars: 500 μm, and 150 μm in the enlarged part. (E) The qPCR results showing the expression of Schwann cell-, axonogenesis-, proliferation-, fibrosis-, and apoptosis-related genes in cryo-T-DRG and cryo-C-DRG. (F) Heatmap of gene expression changes in cryo-T-DRG and cryo-C-DRG before and after cryopreservation. Error bars indicate standard deviations from at least three samples. $^{*}P < 0.05$, $^{**}P < 0.01$, $^{***}P < 0.001$ (Student's *t*-test). C-DRG: Dorsal root ganglia cultured in collagen hydrogel; Cryo-C-DRG: C-DRG after cryopreservation; Cryo-T-DRG: T-DRG after cryopreservation; DAPI: 4′,6-diamidino-2-phenylindole; qPCR: quantitative polymerase chain reaction; T-DRG: dorsal root ganglia cultured on tissue culture plates; TUNEL: terminal deoxynucleotidyl transferase dUTP nick-end labeling.

for 3D culture. Collagen is the main ECM component of nerve tissue. It has favorable mechanical resistance and immunogenicity, and supports cell growth, differentiation, and migration. These properties allow it to be used in various studies in the form of hydrogel (Esteban-Garcia et al., 2020). A previous study by Yu et al. (2010) in an ischemic rat model demonstrated that implanting a collagen hydrogel combined with neural stem cells led to an increase in cell survival, synapse formation, and an improvement in neural function compared with neural stem cells without collagen scaffold. Another major component of ECM is HA. HA is a natural biopolymer that has biocompatibility, biodegradability, and viscoelasticity (Bălașa et al., 2020). It can be found in the ECM of soft connective tissue and body fluids (Menaa et al., 2011), and has potential neuroprotective effects. In one study, HA/methylcellulose hydrogel was injected into a rat model of syringomyelia, eliciting improved tissue and functional responses as well as reduced lipopolysaccharide-mediated microglia activation (Ho et al., 2019). Additionally, the therapeutic efficacy of HA has been demonstrated in stroke management, when neuroglobin-loaded sodium hyaluronate nanoparticles were intravenously injected into rat models and reached the damaged cerebral parenchyma in the early stages (Blanco et al., 2020). Other natural biological materials also have specific advantages. For example, polyvinyl alcohol/gelatin cross-linked hydrogel can be used as a drug carrier

(Imtiaz et al., 2019). Additionally, researchers have studied the effects of dopamine delivery in dextran/gelatin and chitosan/gelatin hydrogels. Both hydrogel types showed the desired effects of drug release, and behavioral and motor improvements were noted in a Parkinson's disease mouse model after treatment (Senthilkumar et al., 2007; Ren et al., 2017). The emerging material graphene has also recently been used for nerve regeneration. Graphene can be chemically modified to control its electrical conductivity, and has been used in combination with cytokines (Menaa et al., 2015). Its property of electrical conductance makes graphene a suitable material for nerve tissue engineering (Bordoni et al., 2020). Some examples of 3D graphene-based scaffolds include so-called graphene foams, which have support the growth and differentiation of neural cells (Ma et al., 2016). Overall, various biomaterials have been applied as 3D scaffolds, and have become an important tool for studying nerve growth and regeneration (Fernandez-Serra et al., 2020).

Schwann cells are important glial cells in DRG, and function to support nerve regeneration, form myelin sheaths, and produce neurotrophic factors (Nascimento et al., 2018). In the present study, we found that DRG in collagen gel expressed high levels of the Schwann cell biomarker S100B. In contrast, the degree of EMT, migration ability, and fibrosis decreased in C-DRG compared with T-DRG. This may be a result of the matrix stiffness of the environment where the cells were cultured. In our previous study, rabbit corneal stromal cells had lower expression of EMT-related genes and exhibited lower degrees of fibrosis and proliferation in collagen hydrogel than in TCP (Cui et al., 2018). After cells and tissue were damaged, EMT enhancement activated cells and increased their proliferation and migration. The same phenomenon has been reported in Schwann cells (Jessen and Arthur-Farraj, 2019). The wound microenvironment can reportedly reprogram Schwann cells into invasive mesenchymal-like cells, to drive peripheral nerve regeneration (Clements et al., 2017). After nerves are injured, EMT-related genes are enriched, and microRNA and long non-coding RNA that regulate EMT are also highly expressed in Schwann cells (Arthur-Farraj et al., 2017). Therefore, DRG cultured in 3D hydrogel may be a more appropriate model than DRG cultured on TCPs when the physiological state of the sensory nerve is studied (Murphy et al., 2017).

Our results suggested that, compared with T-DRG, DRG in collagen hydrogel had better anti-apoptotic abilities. To determine whether this might help to preserve cells during freezing, we analyzed the viability and morphology of DRG after cryopreservation. Our results revealed that cryo-C-DRG were more viable than cryo-T-DRG and had fewer apoptotic cells. Cryopreservation is an effective method for the long-term preservation of tissue and cells. However, tissue and cells are inevitably damaged during the freezing process. When cells undergo a freeze-thaw cycle, osmotic intolerance, cryoprotectant toxicity, and intracellular ice formation may all lead to cell death or loss of function (Woods et al., 2016). After researchers isolate DRG for experiments, the remaining DRG often needs to be cryopreserved to avoid wasting animal resources. Currently, however, cryopreserved DRG often do not have high viability after thawing (Seggio et al., 2008; Schwarz et al., 2019). Thus, our study demonstrated that DRG cryopreserved in collagen hydrogel showed significant improvements in viability and activity compared with TCP cultures. Moreover, axon regeneration in the 3D collagen hydrogel appeared to be guided by Schwann cells, likely because the 3D hydrogel was able to fix the spatial position of the cells. In 2D culture, after cryopreservation and thawing, Schwann cells are often far away from neurons, and provide weak axon guidance and neurotrophic effects. In contrast, Schwann cells are fixed in position in the 3D hydrogel during cryopreservation, which may induce the regeneration of nerve axons and provide neurotrophic factors for neurons after thawing. Compared with traditional culture methods, the transplantation and cryopreservation of tissue engineering materials have obvious advantages. Day et al. (2017) constructed tissue-engineered nerves, and after cryopreservation, Schwann cells helped to guide neuronal regeneration through nerve injury sites. Our previous study also demonstrated that tissue-engineered corneal stroma show good viability after cryopreservation, which facilitates corneal transplantation, as shown by minimal corneal scars after transplantation (Guo et al., 2020).

Although DRG cultured in collagen hydrogel had multiple advantages, there are still problems that need to be solved. The 3D matrix that we used had a single composition (collagen), which is quite different from native tissue ECM, in which different types of ECM components produce different effects on nerve growth. Neural ECM is mostly synthesized by neurons and glial cells. The expression of neural ECM is dynamically regulated during neural development under physiological conditions, and neuronal and glial functions are shaped through a variety of molecular mechanisms (Song and Dityatev, 2018). In the future, a tissue-engineered scaffold with a similar ECM composition to native tissue, with a controllable mechanical microenvironment that mimics physiological and pathological conditions, should be used to construct disease models and transplantable tissue. Moreover, an ideal nerve scaffold should possess sufficient mechanical properties to withstand physiological loads *in vivo*, sufficient biocompatibility without adverse side effects, controllable biodegradation that matches the growth rate of newly formed nerves, specific porosity that permits nutrient and gas transport and blood vessel growth, and the potential to modify and functionalize the scaffold surface (Chiono and Tonda-Turo, 2015). All of these features require a continuous effort to develop more advanced nerve scaffolds.

To conclude, compared with T-DRG, DRG in collagen hydrogel exhibited enhanced neurogenesis and Schwann cell maturation, while EMT and apoptosis were inhibited. After cryopreservation, chicken embryo DRG in collagen hydrogel demonstrated higher viability and reduced levels of fibrosis and apoptosis compared with T-DRG. For the first time, we reported transcriptomic changes in DRG in collagen hydrogel compared with T-DRG, and performed the cryopreservation of DRG in collagen scaffolds. The results demonstrated that *in vitro* cultures of DRG in collagen gel provide a promising approach for the 3D culture, cryopreservation, and transplantation of nerves. Our next step will be to assess the functions of DRG in collagen hydrogel and perform longer cultures. This research provides a reference for the construction, storage, and transportation of tissue-engineered nerves.

Acknowledgments: *We would like to thank Dr. Hon Fai Chan of the School of Biomedical Sciences, the Chinese University of Hong Kong, for help with the revision of the manuscript. We are very grateful to Guangzhou Trauer Biotechnology for providing the collagen solution used in this study.*
Author contributions: *Study concept and design: ZKC, JHM, JSC; literature search: ZKC, SYL, KL, ZJW; experimental studies, data acquisition and analysis, statistical analysis: ZKC, YLG; manuscript preparation: ZKC; manuscript editing: ZKC, JHM, JSC; manuscript review: LST, SBT, JSC. All authors approved the final version of the manuscript.*
Conflicts of interest: *The authors declare that they have no competing interests.*
Financial support: *This study was supported by the National Natural Science Foundation of China, Nos. 82000871 (to ZKC), 81871495 (to JSC); the Natural Science Foundation of Hunan Province, China, No. 2020JJ5001 (to ZKC); the Science Research Grant of Aier Eye Hospital Group, China, No. AF1913D2 (to ZKC), and Central South University Postdoctoral Funds, China. The funders had no roles in the study design, conduction of experiment, data collection and analysis, decision to publish, or preparation of the manuscript.*
Institutional review board statement: *The study was approved by Ethics*

Committee of Aier School of Ophthalmology, Central South University, China (approval No. 2020-IRB16) on March 15, 2020.

Copyright license agreement: *The Copyright License Agreement has been signed by all authors before publication.*

Data sharing statement: *Datasets analyzed during the current study are available from the corresponding author on reasonable request.*

Plagiarism check: *Checked twice by iThenticate.*

Peer review: *Externally peer reviewed.*

Additional files:

Additional Figure 1: *The PCA plot and Pearson correlation heatmap of RNA sequencing samples.*

Additional Figure 2: *Quantitative polymerase chain reaction results of cryo-T-DRG and cryo-C-DRG before and after cryopreservation.*

Additional Table 1: *Information of quantitative polymerase chain reaction primers.*

Additional Table 2: *The original read counts data of RNA sequencing.*

Additional Table 3: *The whole differentially expressed genes.*

Additional Table 4: *The up-regulated GO and KEGG terms.*

Additional Table 5: *The down-regulated GO and KEGG terms.*

References

Arthur-Farraj PJ, Morgan CC, Adamowicz M, Gomez-Sanchez JA, Fazal SV, Beucher A, Razzaghi B, Mirsky R, Jessen KR, Aitman TJ (2017) Changes in the coding and non-coding transcriptome and DNA methylome that define the schwann cell repair phenotype after nerve injury. Cell Rep 20:2719-2734.

Bălașa AF, Chircov C, Grumezescu AM (2020) Marine biocompounds for neuroprotection-a review. Mar Drugs 18:290.

Balasubramanian S, Packard JA, Leach JB, Powell EM (2016) Three-dimensional environment sustains morphological heterogeneity and promotes phenotypic progression during astrocyte development. Tissue Eng Part A 22:885-898.

Blanco S, Peralta S, Morales ME, Martínez-Lara E, Pedrajas JR, Castán H, Peinado M, Ruiz MA (2020) Hyaluronate nanoparticles as a delivery system to carry neuroglobin to the brain after stroke. Pharmaceutics 12:40.

Bordoni M, Scarian E, Rey F, Gagliardi S, Carelli S, Pansarasa O, Cereda C (2020) Biomaterials in neurodegenerative disorders: a promising therapeutic approach. Int J Mol Sci 21:3243.

Chiono V, Tonda-Turo C (2015) Trends in the design of nerve guidance channels in peripheral nerve tissue engineering. Prog Neurobiol 131:87-104.

Clements MP, Byrne E, Camarillo Guerrero LF, Cattin AL, Zakka L, Ashraf A, Burden JJ, Khadayate S, Lloyd AC, Marguerat S, Parrinello S (2017) The wound microenvironment reprograms schwann cells to invasive mesenchymal-like cells to drive peripheral nerve regeneration. Neuron 96:98-114.e7.

Cui Z, Zeng Q, Liu S, Zhang Y, Zhu D, Guo Y, Xie M, Mathew S, Cai D, Zhang J, Chen J (2018) Cell-laden and orthogonal-multilayer tissue-engineered corneal stroma induced by a mechanical collagen microenvironment and transplantation in a rabbit model. Acta Biomater 75:183-199.

Day AGE, Bhangra KS, Murray-Dunning C, Stevanato L, Phillips JB (2017) The effect of hypothermic and cryogenic preservation on engineered neural tissue. Tissue Eng Part C Methods 23:575-582.

de Faria Poloni J, Feltes BC, Bonatto D (2011) Melatonin as a central molecule connecting neural development and calcium signaling. Funct Integr Genomics 11:383-388.

East E, Golding JP, Phillips JB (2009) A versatile 3D culture model facilitates monitoring of astrocytes undergoing reactive gliosis. J Tissue Eng Regen Med 3:634-646.

Esteban-Garcia N, Nombela C, Garrosa J, Rascón-Ramirez FJ, Barcia JA, Sánchez-Sánchez-Rojas L (2020) Neurorestoration approach by biomaterials in ischemic stroke. Front Neurosci 14:431.

Fernandez-Serra R, Gallego R, Lozano P, González-Nieto D (2020) Hydrogels for neuroprotection and functional rewiring: a new era for brain engineering. Neural Regen Res 15:783-789.

Gaudin R, Knipfer C, Henningsen A, Smeets R, Heiland M, Hadlock T (2016) Approaches to peripheral nerve repair: generations of biomaterial conduits yielding to replacing autologous nerve grafts in craniomaxillofacial surgery. Biomed Res Int 2016:3856262.

Gu YW, Li M, Fan ZW, Wang L, Li ZY, Chen S (2018) Physical and chemical properties of 3D extrusive bioprinting cell-encapsulated hydrogel. Zhongguo Zuzhi Gongcheng Yanjiu 22:3583-3588.

Guo Y, Xue Y, Wang P, Cui Z, Cao J, Liu S, Yu Q, Zeng Q, Zhu D, Xie M, Zhang J, Li Z, Liu H, Zhong J, Chen J (2020) Muse cell spheroids have therapeutic effect on corneal scarring wound in mice and tree shrews. Sci Transl Med 12:eaaw1120.

Higgins AZ, Cullen DK, LaPlaca MC, Karlsson JO (2011) Effects of freezing profile parameters on the survival of cryopreserved rat embryonic neural cells. J Neurosci Methods 201:9-16.

Ho MT, Teal CJ, Shoichet MS (2019) A hyaluronan/methylcellulose-based hydrogel for local cell and biomolecule delivery to the central nervous system. Brain Res Bull 148:46-54.

Hopkins AM, De Laporte L, Tortelli F, Spedden E, Staii C, Atherton TJ, Hubbell JA, Kaplan DL (2013) Silk hydrogels as soft substrates for neural tissue engineering. Adv Funct Mater 23:5140-5149.

Imtiaz N, Niazi MBK, Fasim F, Khan BA, Bano SA, Shah GM, Badshah M, Menaa F, Uzair B (2019) Fabrication of an original transparent pva/gelatin hydrogel: in vitro antimicrobial activity against skin pathogens. Int J Polym Sci 2019:7651810.

Jessen KR, Arthur-Farraj P (2019) Repair Schwann cell update: Adaptive reprogramming, EMT, and stemness in regenerating nerves. Glia 67:421-437.

Lan T, Li C, Yang G, Sun Y, Zhuang L, Ou Y, Li H, Wang G, Kisseleva T, Brenner D, Guo J (2018) Sphingosine kinase 1 promotes liver fibrosis by preventing miR-19b-3p-mediated inhibition of CCR2. Hepatology 68:1070-1086.

Ma Q, Yang L, Jiang Z, Song Q, Xiao M, Zhang D, Ma X, Wen T, Cheng G (2016) Three-dimensional stiff graphene scaffold on neural stem cells behavior. ACS Appl Mater Interfaces 8:34227-34233.

Malheiro A, Morgan F, Baker M, Moroni L, Wieringa P (2020) A three-dimensional biomimetic peripheral nerve model for drug testing and disease modelling. Biomaterials 257:120230.

Menaa F, Menaa A, Menaa B (2011) Hyaluronic acid and derivatives for tissue engineering. J Biotechnol Biomaterial S3:001.

Menaa F, Abdelghani A, Menaa B (2015) Graphene nanomaterials as biocompatible and conductive scaffolds for stem cells: impact for tissue engineering and regenerative medicine. J Tissue Eng Regen Med 9:1321-1338.

Mobini S, Song YH, McCrary MW, Schmidt CE (2019) Advances in ex vivo models and lab-on-a-chip devices for neural tissue engineering. Biomaterials 198:146-166.

Moxon SR, Corbett NJ, Fisher K, Potjewyd G, Domingos M, Hooper NM (2019) Blended alginate/collagen hydrogels promote neurogenesis and neuronal maturation. Mater Sci Eng C Mater Biol Appl 104:109904.

Murphy AR, Laslett A, O'Brien CM, Cameron NR (2017) Scaffolds for 3D in vitro culture of neural lineage cells. Acta Biomater 54:1-20.

Nascimento AI, Mar FM, Sousa MM (2018) The intriguing nature of dorsal root ganglion neurons: Linking structure with polarity and function. Prog Neurobiol 168:86-103.

Otto F, Görtz P, Fleischer W, Siebler M (2003) Cryopreserved rat cortical cells develop functional neuronal networks on microelectrode arrays. J Neurosci Methods 128:173-181.

Pardo B, Honegger P (2000) Differentiation of rat striatal embryonic stem cells in vitro: monolayer culture vs. three-dimensional coculture with differentiated brain cells. J Neurosci Res 59:504-512.

Peretz H, Talpalar AE, Vago R, Baranes D (2007) Superior survival and durability of neurons and astrocytes on 3-dimensional aragonite biomatrices. Tissue Eng 13:461-472.

Podda MV, Grassi C (2014) New perspectives in cyclic nucleotide-mediated functions in the CNS: the emerging role of cyclic nucleotide-gated (CNG) channels. Pflugers Arch 466:1241-1257.

Powell S, Vinod A, Lemons ML (2014) Isolation and culture of dissociated sensory neurons from chick embryos. J Vis Exp:51991.

Puopolo M (2019) The hypothalamic-spinal dopaminergic system: a target for pain modulation. Neural Regen Res 14:925-930.

Ren Y, Zhao X, Liang X, Ma PX, Guo B (2017) Injectable hydrogel based on quaternized chitosan, gelatin and dopamine as localized drug delivery system to treat Parkinson's disease. Int J Biol Macromol 105:1079-1087.

Ribeiro A, Vargo S, Powell EM, Leach JB (2012) Substrate three-dimensionality induces elemental morphological transformation of sensory neurons on a physiologic timescale. Tissue Eng Part A 18:93-102.

Robert MC, Juan de Paz L, Graf DA, Gazzin S, Tiribelli C, Bottai H, Rodriguez JV (2016) Cryopreservation by slow cooling of rat neuronal cells. Cryobiology 72:191-197.

Schwarz S, Spitzbarth I, Baumgärtner W, Lehmbecker A (2019) Cryopreservation of canine primary dorsal root ganglion neurons and its impact upon susceptibility to paramyxovirus infection. Int J Mol Sci 20:1058.

Seggio AM, Ellison KS, Hynd MR, Shain W, Thompson DM (2008) Cryopreservation of transfected primary dorsal root ganglia neurons. J Neurosci Methods 173:67-73.

Senthilkumar KS, Saravanan KS, Chandra G, Sindhu KM, Jayakrishnan A, Mohanakumar KP (2007) Unilateral implantation of dopamine-loaded biodegradable hydrogel in the striatum attenuates motor abnormalities in the 6-hydroxydopamine model of hemi-parkinsonism. Behav Brain Res 184:11-18.

Song I, Dityatev A (2018) Crosstalk between glia, extracellular matrix and neurons. Brain Res Bull 136:101-108.

Tay A, Sohrabi A, Poole K, Seidlits S, Di Carlo D (2018) A 3D magnetic hyaluronic acid hydrogel for magnetomechanical neuromodulation of primary dorsal root ganglion neurons. Adv Mater:e1800927.

Tucker T, Riccardi VM, Brown C, Fee J, Sutcliffe M, Vielkind J, Wechsler J, Wolkenstein P, Friedman JM (2011) S100B and neurofibromin immunostaining and X-inactivation patterns of laser-microdissected cells indicate a multicellular origin of some NF1-associated neurofibromas. J Neurosci Res 89:1451-1460.

Varderidou-Minasian S, Verheijen BM, Schätzle P, Hoogenraad CC, Pasterkamp RJ, Altelaar M (2020) Deciphering the proteome dynamics during development of neurons derived from induced pluripotent stem cells. J Proteome Res 19:2391-2403.

Wang S, Ghezzi CE, Gomes R, Pollard RE, Funderburgh JL, Kaplan DL (2017) In vitro 3D corneal tissue model with epithelium, stroma, and innervation. Biomaterials 112:1-9.

Wojtkiewicz DM, Saunders J, Domeshek L, Novak CB, Kaskutas V, Mackinnon SE (2015) Social impact of peripheral nerve injuries. Hand (N Y) 10:161-167.

Woods EJ, Thirumala S, Badhe-Buchanan SS, Clarke D, Mathew AJ (2016) Off the shelf cellular therapeutics: Factors to consider during cryopreservation and storage of human cells for clinical use. Cytotherapy 18:697-711.

Yu H, Cao B, Feng M, Zhou Q, Sun X, Wu S, Jin S, Liu H, Lianhong J (2010) Combinated transplantation of neural stem cells and collagen type I promote functional recovery after cerebral ischemia in rats. Anat Rec (Hoboken) 293:911-917.

Zafeiriou MP, Bao G, Hudson J, Halder R, Blenkle A, Schreiber MK, Fischer A, Schild D, Zimmermann WH (2020) Developmental GABA polarity switch and neuronal plasticity in bioengineered neuronal organoids. Nat Commun 11:3791.

Zhou Y, Zhou B, Pache L, Chang M, Khodabakhshi AH, Tanaseichuk O, Benner C, Chanda SK (2019) Metascape provides a biologist-oriented resource for the analysis of systems-level datasets. Nat Commun 10:1523.

C-Editor: Zhao M; S-Editors: Yu J, Li CH; L-Editors: Gardner B, Yu J, Song CP; T-Editor: Jia Y

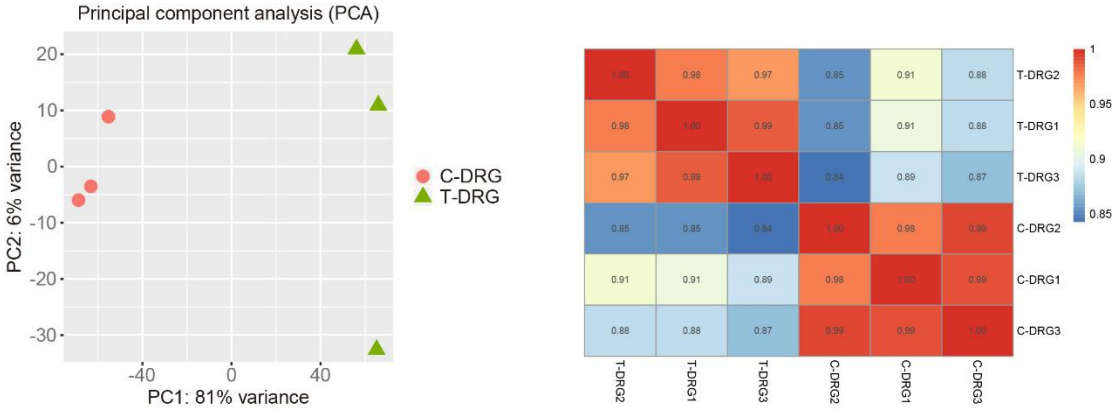

Additional Figure 1 The PCA plot and Pearson correlation heatmap of RNA sequencing samples.

C-DRG: Dorsal root ganglions-laden in collagen hydrogel; PC1: Principal Component 1; PC2: Principal Component 2; PCA: principal components analysis; T-DRG: dorsal root ganglions on tissue culture plate.

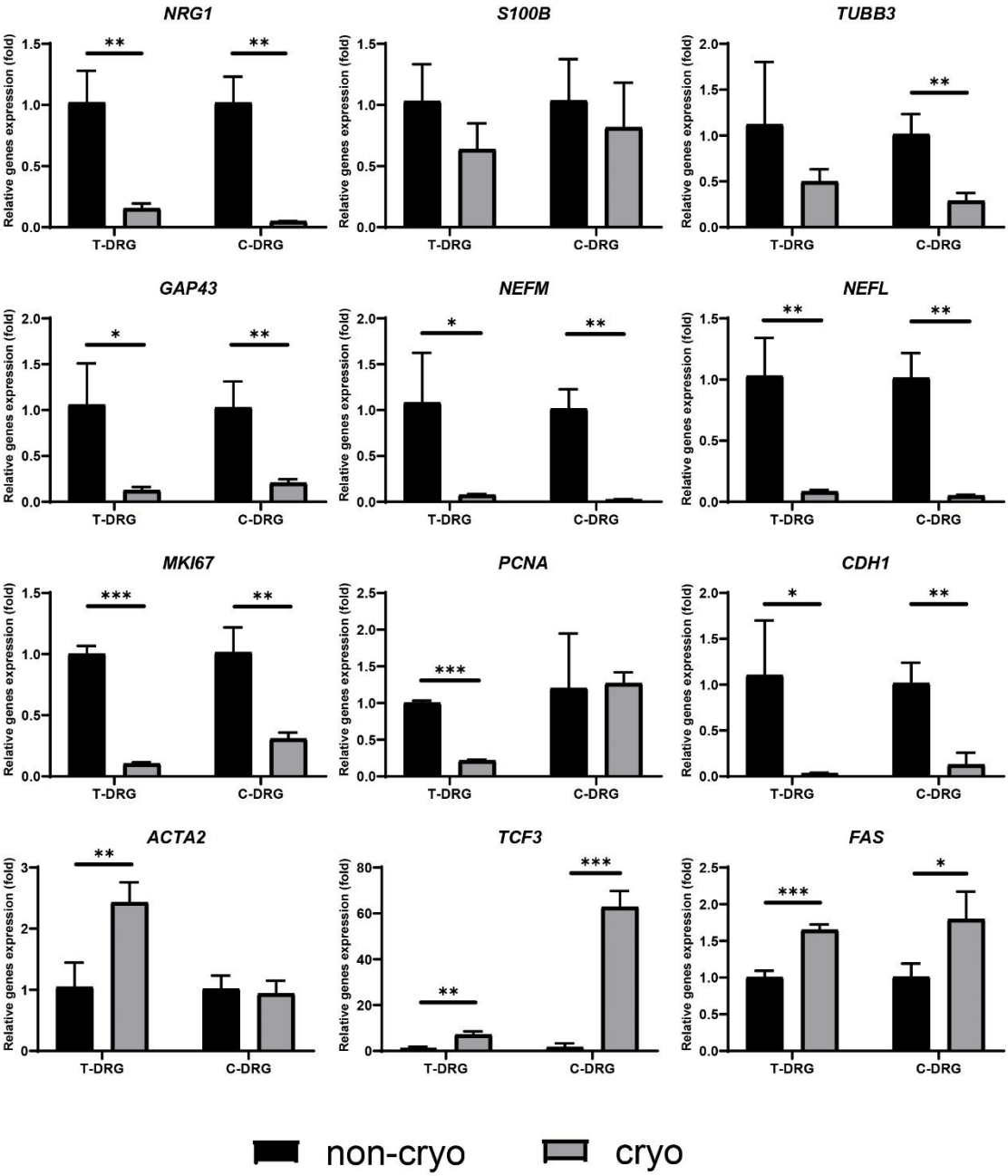

Additional Figure 2 Quantitative polymerase chain reaction results of cryo-T-DRG and cryo-C-DRG before and after cryopreservation.

Error bars indicate SD from at least three samples. *P < 0.05, **P < 0.01, ***P < 0.001 (Student's t-test). C-DRG: Dorsal root ganglions-laden in collagen hydrogel; Cryo-C-DRG: C-DRG after cryopreservation; Cryo-T-DRG: T-DRG after cryopreservation; T-DRG: dorsal root ganglions on tissue culture plate.